LETTERS
PUBLISHED ONLINE: 20 JULY 2014 | DOI: 10.1038/NNANO.2014.135
nature nanotechnology

Explosives detection in a lasing plasmon nanocavity

Ren-Min Ma[1†], Sadao Ota[1†], Yimin Li[1], Sui Yang[1] and Xiang Zhang[1,2*]

Perhaps the most successful application of plasmonics to date has been in sensing, where the interaction of a nanoscale localized field with analytes leads to high-sensitivity detection in real time and in a label-free fashion[1–9]. However, all previous designs have been based on passively excited surface plasmons, in which sensitivity is intrinsically limited by the low quality factors induced by metal losses. It has recently been proposed theoretically that surface plasmon sensors with active excitation (gain-enhanced) can achieve much higher sensitivities due to the amplification of the surface plasmons[10–12]. Here, we experimentally demonstrate an active plasmon sensor that is free of metal losses and operating deep below the diffraction limit for visible light. Loss compensation leads to an intense and sharp lasing emission that is ultrasensitive to adsorbed molecules. We validated the efficacy of our sensor to detect explosives in air under normal conditions and have achieved a sub-part-per-billion detection limit, the lowest reported to date for plasmonic sensors[7,13–18] with 2,4-dinitrotoluene and ammonium nitrate. The selectivity between 2,4-dinitrotoluene, ammonium nitrate and nitrobenzene is on a par with other state-of-the-art explosives detectors[19,20]. Our results show that monitoring the change of the lasing intensity is a superior method than monitoring the wavelength shift, as is widely used in passive surface plasmon sensors. We therefore envisage that nanoscopic sensors that make use of plasmonic lasing could become an important tool in security screening and biomolecular diagnostics.

Cavities in which the light–matter interaction is greatly enhanced have emerged as one of the most promising platforms for sensing[19,21–23]. The sensitivity of these detectors is ultimately determined by the quality factor of the cavity modes and the surface-to-volume ratio, but the diffraction limit of light creates a barrier to improving these two features simultaneously in a conventional optical cavity[23]. Surface plasmons are able to achieve nanoscale confinement of electromagnetic fields, which has led to the development of a variety of surface plasmon-based sensing schemes[1–9]. However, at present, surface plasmon sensors are passively excited and suffer from the intrinsically high ohmic losses of metals, resulting in a low quality factor of the resonances and thus limiting their sensitivity. With active excitation, recently introduced plasmon lasers exhibit well-confined strong local fields, increased radiating power and dramatically narrowed linewidth when compared to passive surface plasmon resonators[24–31]. Such an active plasmon cavity has been theoretically predicted to achieve higher sensitivity to changes in the local environment[10–12].

Figure 1a presents a schematic and Fig. 1b a scanning electron microscope (SEM) image of an active plasmon sensor. The device consists of a single-crystalline semiconductor CdS nanoslab (thickness, 50 nm; length, 600 nm) on top of a Ag surface, separated by an 8-nm-thick MgF_2 gap layer. The surface plasmon effect localizes the electromagnetic field at the interface between the metal and the semiconductor, allowing both the physical size and mode confinement of the device to shrink to the nanometre scale in the dimension perpendicular to the metal surface (Fig. 1c). The calculated mode volume is only $\sim 0.03\lambda^3$ (see Methods). The semiconductor slab, with its atomically smooth surface (Fig. 1d), simultaneously serves as the gain and nanoscale sensing medium in the lasing plasmon nanocavity. The large surface-to-physical-volume ratio (S/V_{phy}) of the nanocavity, which is inversely proportional to the nanoslab thickness, strengthens the surface modulation effect on the emission. The large surface area S favours the adsorption of the analyte, and the small physical volume of active material V_{phy} limits the number of carriers to be modulated inside. In the present device, the estimated number of carriers for the plasmon lasing operation is only $\sim 2 \times 10^4$ (see Methods), making the emission intensity intrinsically sensitive to a very limited number of surface events.

The characterization of device sensitivity was performed in a sealed chamber with two ports for gas exchange and an optical window for both pumping and signal collection (Fig. 2a). The device was exposed to a flow of diluted target chemical at a controlled concentration. 2,4-Dinitrotoluene (DNT) with a saturation concentration of ~100 ppb at room temperature was chosen as the target chemical[19]. Inert N_2 gas was used to dilute the DNT vapour while also serving as the background reference. The device was optically pumped above the lasing threshold at room temperature. Figure 2b shows the dependence between the pump intensity, the emission power and the linewidth of the device. We can see that the lasing emission above threshold has a much narrower linewidth, stronger intensity and higher slope efficiency than those for spontaneous emission. These features endow the device with high performance in terms of its high signal intensity I and relative intensity change $\Delta I/I$ at peak wavelengths.

In our sensing scheme the change in the peak intensity of the lasing emission reflects the detection of molecules adsorbing on the lasing cavity. In Fig. 2c, the lasing emission spectrum under a flow of 8 ppb DNT is compared with that under pure N_2. The surface adsorption of DNT induces an apparent change in the peak intensity at ~505 nm, but no appreciable change in the peak wavelength can be observed. Figure 2d shows the evolution of the peak intensity at 505 nm as the flow alternates between pure N_2 and diluted DNT at various concentrations. We observed an increase in the peak intensity and further saturation within several minutes after switching on a flow of diluted DNT. As shown in Fig. 2d, even at 1 ppb, 6% of $\Delta I/I$ can be detected. The peak intensity decreases to the original value after switching back to a pure-N_2 flow, demonstrating the reversible nature of the response. The response time of the device reflects the slow change of the local DNT concentration at the device surface. This transient time of several minutes is not due to the device itself, but is mainly determined by the flow rate and the volume of the chamber.

We also tracked the lasing peak wavelength via Gaussian fitting of the spectra. There was no appreciable change in the peak

[1]NSF Nanoscale Science and Engineering Centre, 3112 Etcheverry Hall, University of California, Berkeley, California 94720, USA, [2]Materials Sciences Division, Lawrence Berkeley National Laboratory, 1 Cyclotron Road, Berkeley, California 94720, USA, †These authors contributed equally to this work.
*e-mail: xiang@berkeley.edu

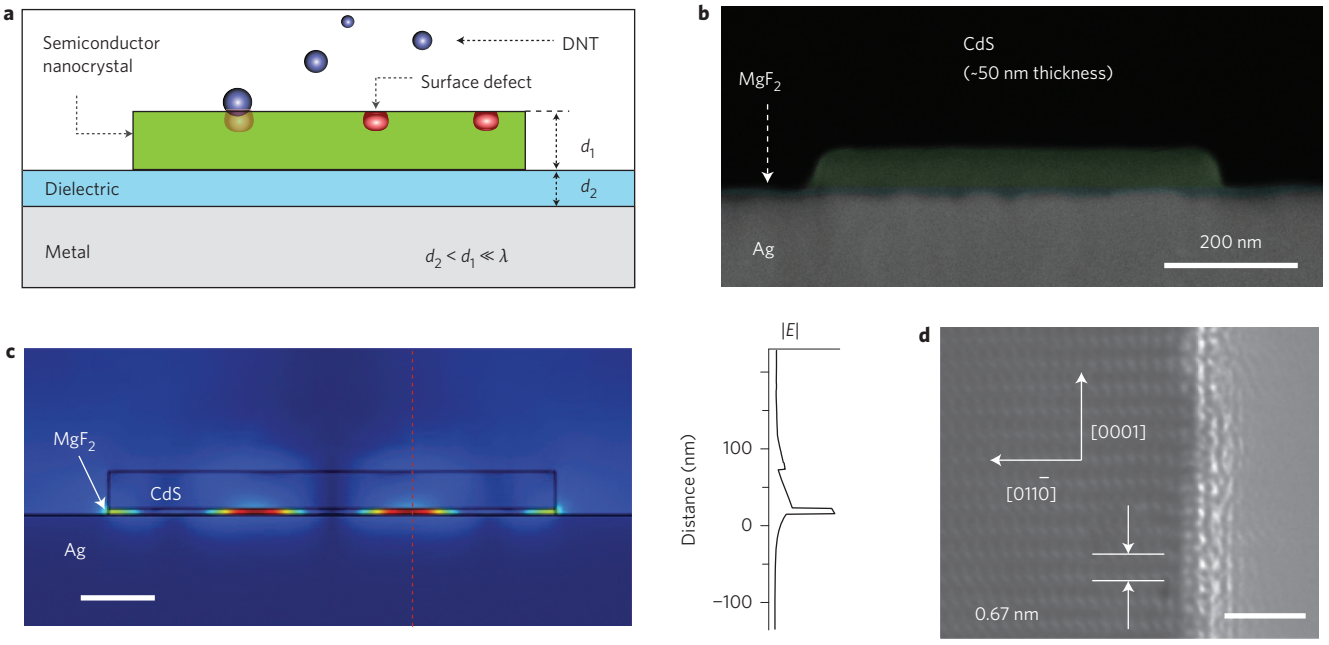

Figure 1 | Schematic, SEM image, simulated field distribution and transmission electron microscope (TEM) image of an active plasmon nanosensor. **a**, Sensing is based on the intensity change in stimulated emission from a lasing plasmon nanocavity with subwavelength electromagnetic field confinement, where the semiconductor slab provides optical gain as well as acts as a sensing material. **b**, SEM image of the device, which consists of a CdS nanoslab (thickness, d_1, 50 nm; length, 600 nm) on top of a Ag film, separated by an 8-nm d_2 low-permittivity MgF_2 layer. **c**, Left: Electric field distribution in a cross-section of the electromagnetic nanoslab cavity mode simulated in three-dimensional space. Scale bar, 100 nm. Right: Electric field amplitude $|E|$ distribution along the dashed red line in the left panel. **d**, High-resolution TEM image (top view) of the CdS slab, showing the single-crystal structure and atomic-level smooth surface, which are crucial for the optical performance of the device. Scale bar, 2 nm. DNT, 2,4-dinitrotoluene.

wavelength at various DNT concentrations (Fig. 2d, green circles). This observation indicates that the direct monitoring of the lasing intensity has a performance superior to that when monitoring the index-change-induced peak wavelength shift in active plasmon sensors.

To understand the underlying mechanism of the sensing process we measured the time-resolved spontaneous emission of the cavity (Fig. 3). For intensity modification there are two possible physical processes[32]. In the first scenario, DNT molecules adsorbed on the device modify the localized charge layer at the surface, giving rise to an electrostatic field in the near-surface region within the semiconductor. In the second scenario, the DNT influences the rate of surface recombination through interactions with surface states. The first process can increase the emission intensity by mitigating band bending, but reduces the emission lifetime because of the increased electron–hole wavefunction overlap. In the second scenario, the adsorbed DNT can reduce the non-radiative recombination by shifting or removing the intrinsic surface state. This process increases the emission intensity and lifetime, as the total emission lifetime τ is dependent on the radiative lifetime τ_{rad} and non-radiative lifetime τ_{nonrad} in the form $1/\tau = 1/\tau_{rad} + 1/\tau_{nonrad}$. In the experiment we delivered 100 ppb DNT vapour into the chamber. The results show that the emission intensity from the device increased after introduction of the vapour, following the same trend as the stimulated emission regime. Meanwhile, the measured emission lifetime became longer, as shown in Fig. 3. These results suggest that our detection mechanism relies mainly on surface recombination velocity modification.

Although the detection of DNT in N_2 has proved the principle of our sensor devices, achieving a practical sensor requires measuring the target molecules in air in the presence of common interferences. To achieve this, we alternately delivered air (comprising N_2, O_2, H_2O, CO_2, CO, total hydrocarbon, NO_x and so on) and N_2 into the chamber. The lasing intensities increased by only ~1% after each air delivery, then decreased to the original value after switching back to pure N_2. We then conducted a series of experiments to detect three different explosive molecules: DNT, ammonium nitrate (AN) and nitrobenzene (NB). Air was used both to dilute them and as the background reference. Figure 4a–c presents continuous traces of lasing intensities with varied concentrations of these analytes. The lasing intensities clearly increase after each analyte delivery and decrease to the initial value after switching the input gas to air only.

The calibration curves for the three analytes were obtained from the sensor responses, with $\Delta I/I$ plotted as a function of the analyte vapour concentrations (Fig. 4d). The sensitivities (defined as the slope of the calibration curves[33]) for DNT, AN and NB are 1.2%/ppb, 6.1%/ppb and 0.4%/ppm, respectively. The limits of detection of these analytes in air can also be obtained from the calibration curves. The minimum distinguishable analytical signal S_{lod} is taken as $a + 3S$, where a and S are the y-intercept and standard deviation of the regression of the calibration curves, respectively. The detection limits obtained for DNT, AN and NB are 0.67 ppb, 0.4 ppb and 7.2 ppm, respectively. We have therefore demonstrated that our sensor responds to the different analytes in air with good robustness, reversibility, as well as stability over our long-lasting experiments (>5 h). Note that our sensor is based on the surface recombination velocity modification, which is sensitive to the electron deficiency of adsorbed molecules. Our device can identify different explosive traces with distinct sensitivity when only one explosive is present in air. However, distinguishing each type of explosive in a mix of multiple explosives remains a challenging task. Nevertheless, in field applications such as airports, detecting explosives of any kind in air is sufficiently useful as a first alarm, even without distinguishing them. Further work, such as using a sensor matrix, coating with appropriate functional molecules or utilizing the enhanced Raman signal in the lasing plasmon sensor, will be needed to further explore the specific response of an analyte.

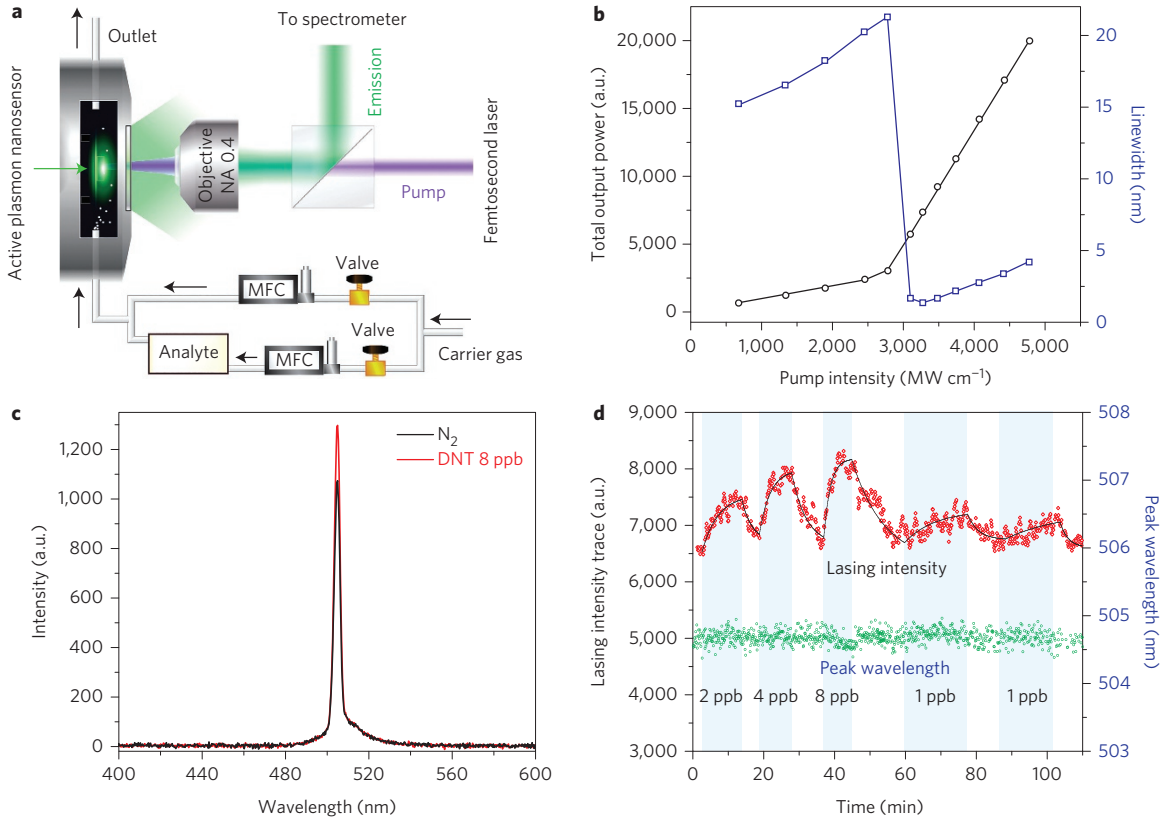

Figure 2 | Characterization of the active plasmon sensor. a, Experimental set-up. The device is placed in a sealed chamber, with two ports for gas exchange controlled by mass flow controllers (MFCs), and an optical window for both pumping and signal collection. **b**, Pump intensity dependence of the total output power and linewidth of the device. The stimulated emission above the lasing threshold has stronger intensity, higher slope and much narrower linewidth than the spontaneous emission. **c**, Measured spectra of the lasing plasmon cavity under N_2 and 8 ppb 2,4-dinitrotoluene (DNT). **d**, Red diamond: continuous trace of emission intensities of the active plasmon nanosensor when delivering DNT vapour at concentrations of 1, 2, 4 and 8 ppb. Black line: guide to the eye. Green circles: the tracked lasing peak wavelength obtained by Gaussian fitting of the spectra. There is no appreciable change in the peak wavelength at various DNT concentrations, which indicates that directly monitoring the lasing intensity has superior performance than monitoring the index-change-induced peak wavelength shift in active plasmon sensors.

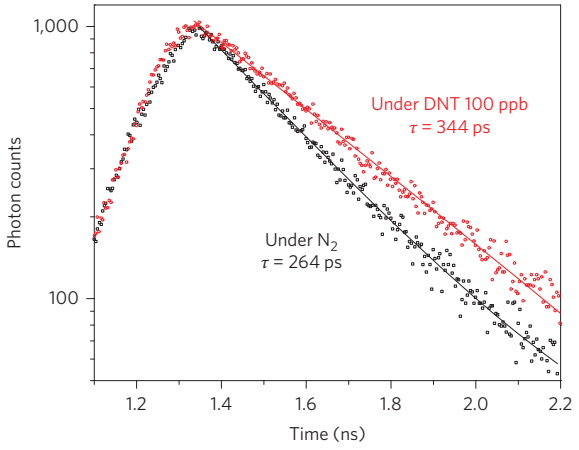

Figure 3 | Time-resolved emission of the sensor measured at the spontaneous emission region to investigate dynamic processes of the photon-excited carrier relaxation. Two typical time-resolved spontaneous emissions under N_2 and 100 ppb 2,4-dinitrotoluene (DNT). After the introduction of DNT vapour, the emission intensity from the device increased, following the same trend as the stimulated emission region. Meanwhile, the measured emission lifetime became longer. Both the intensity and lifetime changes to the spontaneous emission with DNT suggest that the intensity increase is mainly due to the surface recombination velocity modification.

The sensitivity of our sensor in the lasing condition is significantly enhanced when compared to that in the spontaneous emission condition. Figure 5a shows the continuous trace of spontaneous emission intensities when DNT was delivered as vapour of varied concentration. Figure 5b shows the calibration curves for DNT detection in the spontaneous emission condition. The sensitivity and detection limit were obtained as 0.23%/ppb and 14 ppb, respectively. We can see that the sensitivity of lasing emission is approximately five times higher than that of spontaneous emission, and the detection limit is about 21 times better. We note that the peak intensity of the lasing emission is about 60 times higher than that of the spontaneous emission (Fig. 5c). So, the sensitivity of lasing emission is about 300 times higher than that of spontaneous emission when ΔI is directly used as the measure of signal[19].

In summary, we have experimentally demonstrated the first active plasmon sensor with sub-part-per-billion-level explosive molecule detection. We can make the following observations. First, the solid-state semiconductor simultaneously provides optical gain and acts as the sensing medium in our active plasmon sensors, and the devices detect different explosive molecules with specific responses depending on the electron deficiencies of the molecules. Second, the sensitivity of the lasing emission from the calibration curve is about 300 times greater than that of spontaneous emission, because the lasing emission has a much stronger intensity and higher slope efficiency. Finally, directly monitoring the lasing intensity has a superior performance than monitoring the wavelength shift due

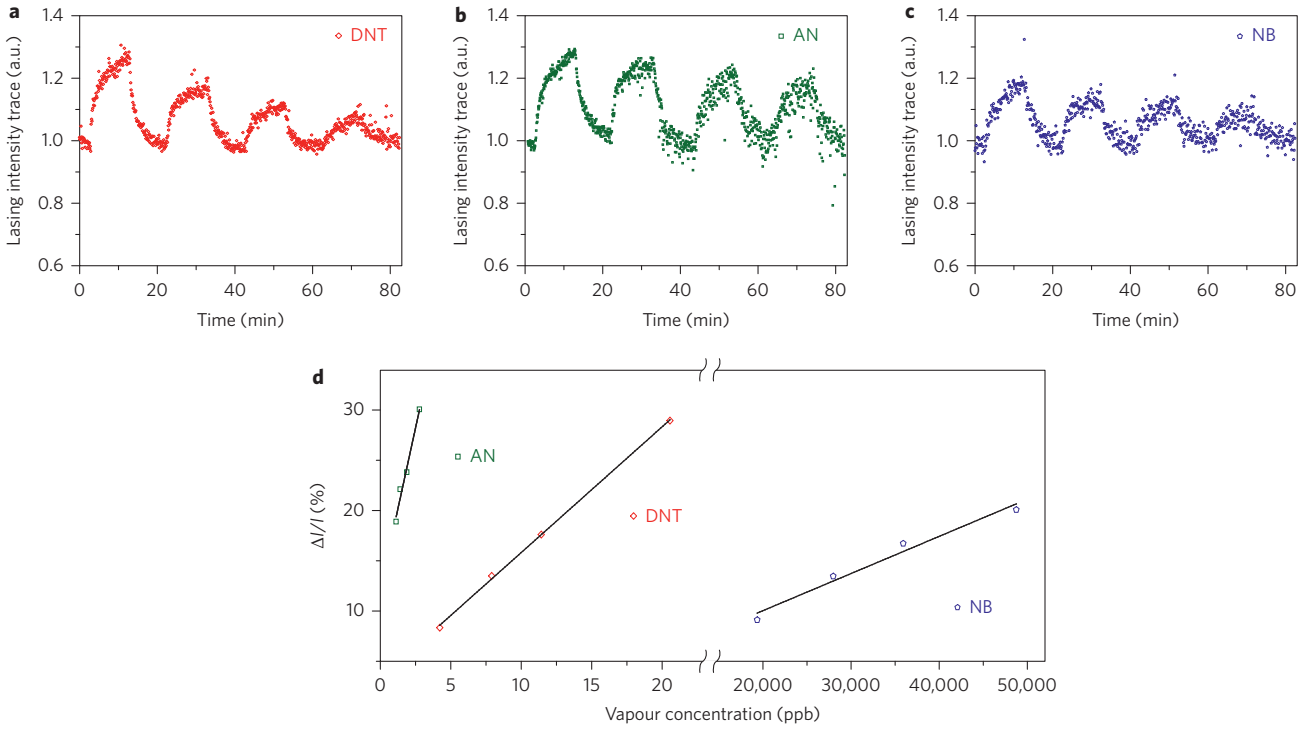

Figure 4 | Detection of 2,4-dinitrotoluene, ammonium nitrate and nitrobenzene in air. a–c, Continuous traces of lasing intensities at different vapour concentrations of DNT (**a**), AN (**b**) and NB (**c**), diluted by air. **d**, Calibration curves for the three analytes. The sensitivities defined as the slope of the calibration curves for DNT, AN and NB are 1.2%/ppb, 6.1%/ppb and 0.4%/ppm, respectively. The detection limits obtained for DNT, AN and NB are 0.67 ppb, 0.4 ppb and 7.2 ppm, respectively. The device has a specific response to different target molecules depending on their specific electron deficiencies, because our sensing is mainly based on the surface recombination velocity modification, which is sensitive to the electron deficiency of adsorbed molecules.

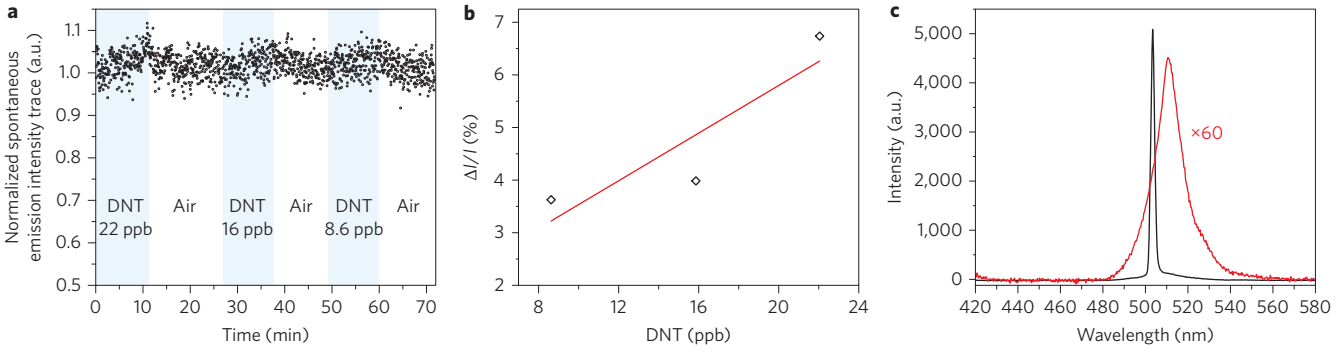

Figure 5 | Detection of explosive molecules via spontaneous emission. a, Continuous trace of spontaneous emission intensities at different 2,4-dinitrotoluene (DNT) vapour concentrations diluted by air. **b**, Calibration curve for DNT detection via spontaneous emission. The sensitivity and detection limit are ~0.23%/ppb and ~14 ppb, respectively. **c**, Spontaneous emission and lasing emission of the sensor device studied in Figs 4 and 5. When ΔI is used as a direct measure of the signal, the sensitivity of lasing emission is approximately 300 times higher than that of spontaneous emission.

to the index change. The wavelength shift was hardly distinguishable in the ultra-trace detection. These results demonstrate the potential of actively excited surface plasmons for chemical sensing, with important implications for security, defence and other applications.

Methods

Sample preparation. The CdS nanoslabs were synthesized using a chemical vapour deposition method. CdS (99.995%) powders were used as the source, and pieces of Si wafers covered with 10-nm-thick thermally evaporated Au catalysts were used as the substrates. The as-grown CdS nanoslabs had a single-crystalline lattice structure with a lattice spacing of $a_{CdS} = 0.67$ nm along the [0001] axis, corresponding to a wurzite crystal lattice (Fig. 1b). The Ag/MgF_2 substrates were deposited by electron-beam evaporation. The film roughness (root mean square) measured by atomic force microscopy was ~1 nm. CdS nanoslabs were deposited from solution by spin-coating onto the Ag/MgF_2 substrates.

Numerical mode simulations. The optical modes of the active plasmon sensors were calculated using a finite-element method three-dimensional eigenmode solver (Comsol Multiphysics). In this model, the CdS nanoslab ($n_{CdS} = 2.5$) lies in contact with an 8 nm MgF_2 ($n_{MgF_2} = 1.38$) gap layer above a single Ag strip ($\varepsilon_{Ag} = \varepsilon_b - E_P^2[E(E - i\gamma)]^{-1}$, $\varepsilon_b = 5$ eV, $\gamma = 0.04$ eV). The effective mode volume of the lasing plasmon cavity is calculated as $V_{eff} = \left(\int w_{em}(\mathbf{r}) d^3\mathbf{r} / \varepsilon_0 \varepsilon(|\mathbf{E}|^2_{max}) \right)$, where w_{em} is the electromagnetic energy density of the mode $\mathbf{E}$ in the denominator is the evaluated maximal electric field. Taking into account the strongly dispersive property of Ag, $w_{em}(\mathbf{r})$ is equal to $(1/2)\left[\mathrm{Re}\left[d(\omega\varepsilon)/d\omega\right]|\mathbf{E}(\mathbf{r})|^2 + \mu|\mathbf{H}(\mathbf{r})|^2\right]$. The Q factors of the cavity modes are calculated from the formula $Q = f_r/\Delta f$, where f_r is the resonance frequency and Δf is the full-width at half-maximum of the resonance spectrum. For the Q factors of the cavity modes with introduced gain, a complex refractive index of $n_{CdS} = n - i\kappa$ is set, where the gain coefficient κ can vary depending on the pump intensity. The Q factor is significantly enhanced by orders of magnitude with increasing gain coefficient κ, and reaches a maximum at $\kappa = 0.19$, which corresponds to a material gain ($g = 4\pi\kappa/\lambda$) of ~9,500 cm^{-1}.

Device measurement. The active plasmon nanosensors were placed in a sealed chamber. The saturated DNT vapour in N_2 was diluted by another N_2 channel, so its final concentration could be determined by the ratio of the flow rates in the two channels. The devices were optically pumped by a frequency-doubled, mode-locked Ti:sapphire laser (Spectra Physics) with $\lambda_{pump} = 405$ nm, a 10 kHz repetition rate and ~100 fs pulse length. A ×20 objective lens (NA = 0.4) was used to focus the pump beam to a ~2-μm-diameter spot onto the sample and collect the luminescence. All experiments were conducted at room temperature.

Cavity carrier number estimation. The large surface-to-physical-volume ratio (S/V_{phy}) of the nanocavity strengthens the surface modulation effect, because the number of carriers inside is essentially limited by V_{phy} and there is a large surface area for analyte absorption. S/V_{phy} can also be expressed as $(S \cdot n_e/N)$, where $V_{phy} = (N/n_e)$, n_e is the carrier concentration and N is the carrier number in the cavity. The carrier density around the lasing threshold of the plasmon nanoslab cavity is on the order of 1×10^{18} cm^{-3} (ref. 31). Given that the V_{phy} of the CdS nanoslab is ~0.018 μm^3 (~0.14λ^3), the number of carriers for lasing operations (N) in the device is ~1.8×10^4.

Received 5 August 2013; accepted 6 April 2014; published online 20 July 2014

References

1. Peng, G. *et al.* Diagnosing lung cancer in exhaled breath using gold nanoparticles. *Nature Nanotech.* **4,** 669–673 (2009).
2. Liu, N., Tang, M. L., Hentschel, M., Giessen, H. & Alivisatos, A. P. Nanoantenna-enhanced gas sensing in a single tailored nanofocus. *Nature Mater.* **10,** 631–636 (2011).
3. Anker, J. N. *et al.* Biosensing with plasmonic nanosensors. *Nature Mater.* **7,** 442–453 (2008).
4. Kabashin, A. V. *et al.* Plasmonic nanorod metamaterials for biosensing. *Nature Mater.* **8,** 867–871 (2009).
5. Cubukcu, E., Zhang, S., Park, Y-S., Bartal, G. & Zhang, X. Split ring resonator sensors for infrared detection of single molecular monolayers. *Appl. Phys. Lett.* **95,** 043113 (2009).
6. Li, J. F. *et al.* Shell-isolated nanoparticle-enhanced Raman spectroscopy. *Nature* **464,** 392–395 (2010).
7. Mayer, K. M. & Hafner, J. H. Localized surface plasmon resonance sensors. *Chem. Rev.* **111,** 3828–3857 (2011).
8. Yanika, A. A. *et al.* Seeing protein monolayers with the naked eye through plasmonic Fano resonances. *Proc. Natl Acad. Sci. USA* **108,** 11784–11789 (2011).
9. Brolo, A. G. Plasmonics for future biosensors. *Nature Photon.* **6,** 709–713 (2012).
10. Lawandy, N. M. Localized surface plasmon singularities in amplifying media. *Appl. Phys. Lett.* **85,** 5040–5042 (2004).
11. Gordon, J. A. & Ziolkowski, R. W. Investigating functionalized active coated nanoparticles for use in nano-sensing applications. *Opt. Express* **15,** 12562–12582 (2007).
12. Li, Z-Y. & Xia, Y. Metal nanoparticles with gain toward single-molecule detection by surface-enhanced Raman scattering. *Nano Lett.* **10,** 243–249 (2010).
13. Piorek, B. D., Lee, S. J., Moskovits, M. & Meinhart, C. D. Free-surface microfluidics/surface-enhanced Raman spectroscopy for real-time trace vapor detection of explosives. *Anal. Chem.* **84,** 9700–9705 (2012).
14. Sylvia, J. M., Janni, J. A., Klein, J. D. & Spencer, K. M. Surface-enhanced Raman detection of 2,4-dinitrotoluene impurity vapor as a marker to locate landmines. *Anal. Chem.* **72,** 5834–5840 (2000).
15. Khaing Oo, M. K., Chang, C-F., Sun, Y. & Fan, X. Rapid, sensitive DNT vapor detection with UV-assisted photo-chemically synthesized gold nanoparticle SERS substrates. *Analyst* **136,** 2811–2817 (2011).
16. Bowen, J. *et al.* Gas-phase detection of trinitrotoluene utilizing a solid-phase antibody immobilized on a gold film by means of surface plasmon resonance spectroscopy. *Appl. Spectrosc.* **57,** 906–914 (2003).
17. Baker, G. A. & Moore, D. S. Progress in plasmonic engineering of surface-enhanced Raman-scattering substrates toward ultra-trace analysis. *Anal. Bioanal. Chem.* **382,** 1751–1770 (2005).
18. Tamane, S., Topal, C. & Kalkan, A. J. Vapor phase SERS sensor for explosives detection. *Proceedings of the 11th IEEE International Conference on Nanotechnology* 301–306 (2011).
19. Rose, A., Zhu, Z., Madigan, C. F., Swager, T. M. & Bulovic, V. Sensitivity gains in chemosensing by lasing action in organic polymers. *Nature* **434,** 876–879 (2005).
20. Rochat, S. & Swager, T. M. Conjugated amplifying polymers for optical sensing applications. *ACS Appl. Mater. Interfaces* **5,** 4488–4502 (2013).
21. He, L., Ozdemir, S. K., Zhu, J., Kim, W. & Yang, L. Detecting single viruses and nanoparticles using whispering gallery microlasers. *Nature Nanotech.* **6,** 428–432 (2011).
22. Vahala, K. J. Optical microcavities. *Nature* **424,** 839–846 (2003).
23. Vollmer, F. & Arnold, S. Whispering-gallery-mode biosensing: label-free detection down to single molecules. *Nature Methods* **5,** 591–596 (2008).
24. Bergman, D. J. & Stockman, M. I. Surface plasmon amplification by stimulated emission of radiation: quantum generation of coherent surface plasmons in nanosystems. *Phys. Rev. Lett.* **90,** 027402 (2003).
25. Hill, M. T. *et al.* Lasing in metal–insulator–metal sub-wavelength plasmonic waveguides. *Opt. Express* **17,** 11107–11112 (2009).
26. Noginov, M. A. *et al.* Demonstration of a spaser-based nanolaser. *Nature* **460,** 1110–1113 (2009).
27. Oulton, R. F. *et al.* Plasmon lasers at deep subwavelength scale. *Nature* **461,** 629–632 (2009).
28. Ma, R-M., Oulton, R. F., Sorger, V. J., Bartal, G. & Zhang, X. Room temperature sub-diffraction-limited plasmon laser by total internal reflection. *Nature Mater.* **10,** 110–113 (2011).
29. Khajavikhan, M. *et al.* Thresholdless nanoscale coaxial lasers. *Nature* **482,** 204–207 (2012).
30. Lu, Y-J. *et al.* Plasmonic nanolaser using epitaxially grown silver film. *Science* **337,** 450–453 (2012).
31. Ma, R-M., Yin, X. B., Oulton, R. F., Sorger, V. J. & Zhang, X. Multiplexed and electrically modulated plasmon laser circuit. *Nano Lett.* **12,** 5396–5402 (2012).
32. Seker, F., Meeker, K., Kuech, T. F. & Ellis, A. B. Surface chemistry of prototypical bulk II–VI and III–V semiconductors and implications for chemical sensing. *Chem. Rev.* **100,** 2505–2536 (2000).
33. Skoog, D. A., Holler, F. J. & Crouch, S. R. *Principles of Instrumental Analysis* 6th edn (Thomson Learning, 2006).

Acknowledgements

The authors acknowledge financial support from the US Air Force Office of Scientific Research (AFOSR, grant no. FA9550-12-1-0197).

Author contributions

R-M.M. conducted theoretical simulations. R-M.M. and S.O. performed device fabrication and optical measurements. R-M.M. and S.O. wrote the manuscript. All authors discussed the results and contributed to the manuscript revision. X.Z. guided the research.

Additional information

Reprints and permissions information is available online at www.nature.com/reprints. Correspondence and requests for materials should be addressed to X.Z.

Competing financial interests

The authors declare no competing financial interests.